Environmental Science and Pollution Research
https://doi.org/10.1007/s11356-021-15612-9

RESEARCH ARTICLE

Synthesis of novel hierarchical micro/nanostructures AlOOH/AlFe and their application for As(V) removal

Natalia Svarovskaya[1] · Olga Bakina[1] · Elena Glazkova[1] · Nikolay Rodkevich[1] · Marat Lerner[1] · Ekaterina Vornakova[1] · Valeria Chzhou[1] · Liudmila Naumova[2]

Received: 14 March 2021 / Accepted: 19 July 2021

Abstract

Hierarchical micro/nanostructured composites, which contain iron and/or its (hydr)oxides, demonstrate high rate and capacity of arsenic adsorption. The main objective of this paper is the use of novel low toxicity AlOOH/AlFe hierarchical micro/nanostructures for arsenic removal. AlOOH/AlFe composite was obtained by simple water oxidation in mild conditions using AlFe bimetallic nanopowder as a precursor. AlFe bimetallic nanopowder was produced by electrical explosive of two twisted wires in argon atmosphere. The productivity of the electrical explosion assembly was 50 g/h, with the consumption of the electrical energy was 75 kW·h/kg. AlFe bimetallic nanoparticles were chemically active and interacted with water at 60 °C. This nanocomposite AlOOH/AlFe is low cost and adsorbs more than 200 mg/g As(V) from its aqueous solution. AlOOH/AlFe composite has flower-like morphology and specific surface area 247.1 m^2/g. The phase composition of nanostructures is present AlOOH boehmite and AlFe intermetallic compound. AlOOH/AlFe composite was not previously used for this. The flower-shape AlOOH morphology not only facilitated deliverability, but increased the As(V) sorption capacity by up to 200 mg/g. The adsorption kinetics has been found to be described by a pseudo-second-order equation of Lagergren and Weber-Morris models while the experimental adsorption isotherm is closest to the Freundlich model. This indicates the energy heterogeneity of the adsorbent surface and multilayer adsorption. The use of non-toxic nanostructures opens up new options to treat water affected by arsenic pollution.

Keywords Bimetallic nanoparticles · Nanocomposites · Hierarchical micro/nanostructures · Arsenic adsorption

Introduction

Adsorption is perfect water treatment method due to its ease of operation, the availability of a wide range of adsorbents, cost efficiency, and sludge-free operation (Ali 2012). Nanoparticles have proven to be excellent adsorbents due to their unique properties. The most important property of the nanoparticles is high surface area which provides high adsorption rate and high adsorption capacity. However, nanoparticles show an inherent tendency toward agglomeration due to their high surface energy reducing effective surface area, difficulty to separate spent nanoparticles adsorbent from aqueous medium (Habuda-Stanić and Nujić 2015).

To overcome the challenges allows the use of nanostructured materials. Hierarchical micro/nanostructured materials which are nanoparticles particularly assembled into microstructures have been actively studied in the last decade. Morphology of the micro/nanostructured material defines complex of the properties characteristic for effective adsorbent

Highlights
- Composite nanostructures were synthesized by simple water oxidation in mild conditions using AlFe bimetallic nanopowder as a precursor.
- The nanostructures were characterized using EDS, XRD, TEM, SEM, and BET.
- The adsorption behavior of the nanostructures was studied using kinetic and adsorption isotherm experiments.
- Described the improvements for adsorption of arsenic using AlOOH/AlFe composite nanostructures.

Responsible Editor: Ioannis A. Katsoyiannis

✉ Olga Bakina
ovbakina@ispms.tsc.ru

[1] Institute of Strength Physics and Materials Science of Siberian Branch Russian Academy of Sciences (ISPMS SB RAS), 8/2 Akademicheskii pr, Tomsk 634050, Russia

[2] National Research Tomsk State University, 36 Lenin Ave, Tomsk 634050, Russia

Published online: 05 August 2021

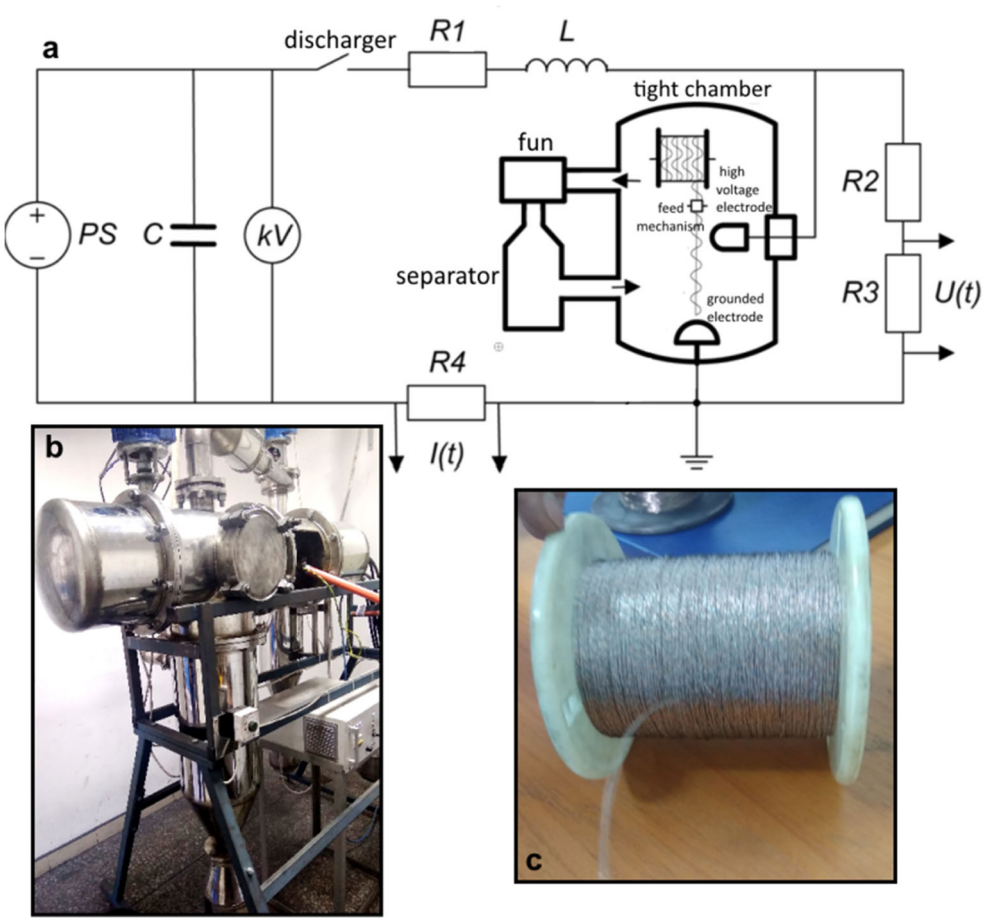

Fig. 1 Electric circuit diagram (**a**), photograph of EEW device (**b**), and spool with two twisted wires (**c**)

with main being high specific surface available for adsorbates of various sizes due to open pore structure, resistance to agglomeration, and stability of properties. This defines their use in the field of environmental protection, in particular, for water purification (Ren et al. 2013; Cai et al. 2014).

Arsenic is one of the most important contaminants with high toxicity in natural water and soil systems worldwide (Shakoor et al. 2017). A large number of methods are currently used to remove arsenic from water and soil, such as ion exchange, phytoremediation, adsorption, phytobial remediation, chemical precipitation, electrokinetic methods, and electrocoagulation (Alka et al. 2020). Adsorption methods are currently the most widely used for removing As from water and soil. The adsorbents have significant advantages such as secure operation handling, flexibility, low cost, sludge-free, and high removal efficiency (Yılmaz et al. 2018; Ecer et al. 2018). Materials containing compounds of iron, which has a high affinity for arsenic and forms insoluble compounds, are commonly used to remove arsenic. In addition, iron-containing sorbents are suitable for magnetic separation due to their magnetic properties (Kumar and Jiang 2017). Effective adsorbents are iron-containing nanoparticles providing high removal rate and high adsorption capacity (Habuda-Stanić and Nujić 2015). However, one of the major disadvantages is that adsorbents have a low specific surface area when using in the form of metal oxides.

The improved porous structure is obtained by depositing iron or iron oxide nanoparticles on porous substrates — zeolite (Li et al. 2018), mesoporous molecular sieve SBA-15 (Peng et al. 2018), polystyrene microspheres with a shell of reduced graphene oxide and graphene oxide (Kang et al. 2017), and macrogel of graphene oxide, modified with polydopamine (Guo et al. 2015). Adsorption of As was improved using double oxides and hydroxides of iron with other elements — Mg (Guo et al. 2017), Mn (Martinez–Vargas et al. 2018; Zhong et al. 2018), and Zn (Zhu et al. 2018). Eslami et al. (2019a, 2019b, 2020) synthesized Fe_2O_3-Mn_2O_3 nanocomposite for As(V) removal with high efficiency and low cost. We consider aluminum to be preferable because alumina is an effective adsorbent and can be synthesized in the form of a nanoflowers or urchin-like hierarchical micro/nanomaterials (Dubey et al. 2017). Synergetic adsorption was observed using nanocomposites from iron and aluminum oxides obtained by the hydrothermal method (Li et al. 2013; Mikhaylov et al. 2017).

Many methods are used to obtain composites based on iron oxide composites on, such as new aeration co-precipitation method (Eslami et al. 2018, 2019a, 2019b), green synthesis (Zhang et al. 2020), and sonochemical

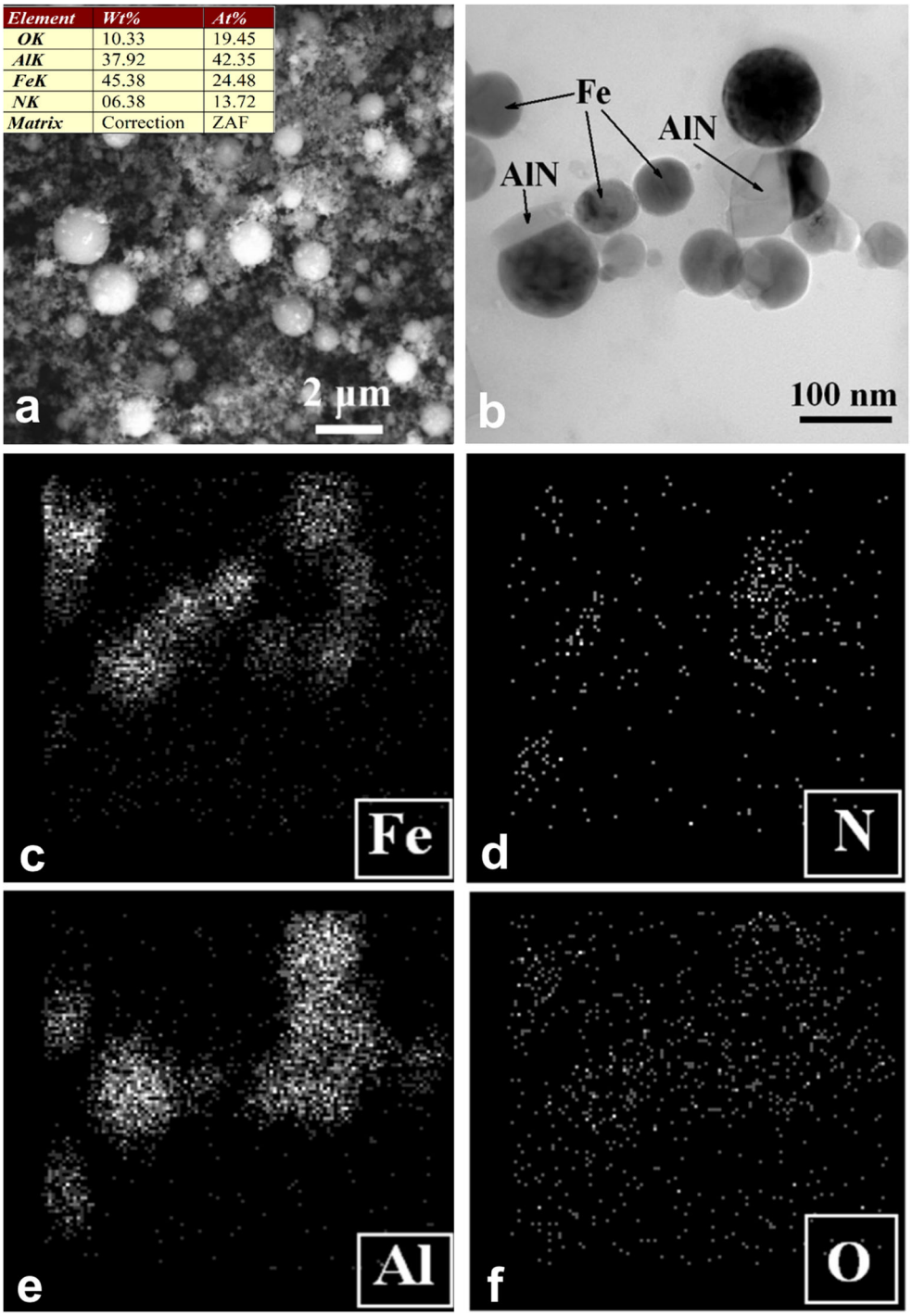

Fig. 2 SEM (**a**), TEM (**b**), EDX mapping showing iron, nitrogen, aluminum, and oxygen distributions in Al/Fe(N_2) nanoparticles and EDS spectrum of Al/Fe(N_2) nanopowder (**c**, **d**, **e**, **f**)

and radiochemical processes (Seino et al. 2006). A promising method for the synthesis of chemical active metal nanoparticles is an electric explosion of wire (EEW). EEW is an effective, environmentally friendly, and high-performance method based on the atomization of a thin metal wire in a gas by a high current pulse. Early we described the simple synthesis of flower-shape pseudoboehmite nanopetals by AlN/Al composite nanoparticles water oxidation at 60 °C (Bakina et al. 2015).

In the present study, a new hierarchical micro/nanostructured flower-like composite AlOOH/AlFe has been synthesized successfully by a simple, one-pot method under mild conditions using only water and a precursor — Al/Fe(N_2) nanopowder and then the physicochemical, structural, and adsorption properties of the nanocomposite were studied by several techniques. As(V) was used as target pollutant. As per the author's knowledge, this novel composite has never been reported for arsenic removal.

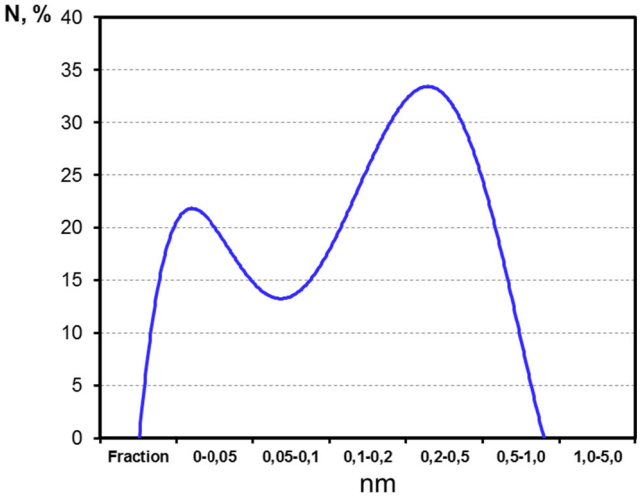

Fig. 3 Agglomerates of nanoparticle size distribution (CPS 24000, CPS Disk Instruments)

Materials and methods

Materials

Composite iron-aluminum bimetallic Al/Fe(N_2) nanoparticles were obtained by electric explosion of two twisted aluminum and iron wires in a nitrogen atmosphere, the pressure of the gas mixture being 3×10^5 Pa. Electric circuit diagram and photograph of EEW device for production the nanoparticles are given in Fig 1. The detailed description of the EEW processing of bimetallic nanoparticles can be found (Lerner et al. 2016). Iron wire with the diameter d = 0.20 mm and aluminum wire with the diameter d = 0.35 mm, both 90-mm long, were used for electric explosion. The atomic ratio of Fe-to-Al in the wires was around 50 wt% Fe and 50 wt% Al. The capacitance of the capacitor bank (C) and the charging voltage (U) were 2.8 μF and 26 kV, respectively. Nanopowders are pyrophoric just after preparation and they are passivated by slow letting-to-air method before use. Analytical grade sodium arsenate Na_3AsO_4 was used without additional purification. The water used was prepared by reverse osmosis method.

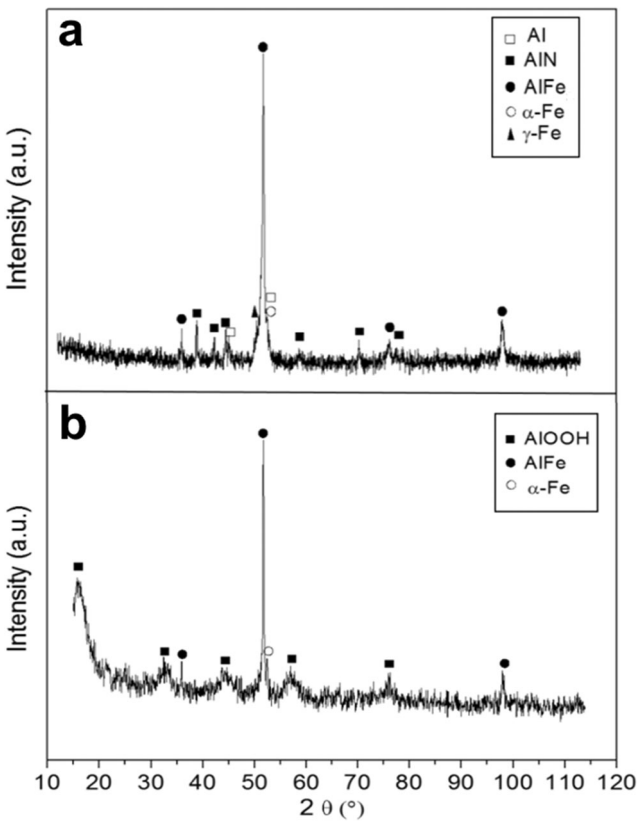

Fig. 4 XRD patterns of Al/Fe(N_2) nanopowder before (**a**) and after (**b**) reaction with water at 60 °C

Nanopowder characterization

The nanoparticles prepared were characterized by transmission electron microscopy (TEM) (JEM-2100, JEOL, Japan) with integrated energy-dispersive X-ray spectroscopy (EDS) system X-Max (Oxford Instruments, GB), scanning electron microscopy (SEM) (LEO EVO 50), and *X-ray diffraction (XRD) (Shimadzu XRD 6000* diffractometer). The specific surface area and texture of the AlOOH/AlFe micro/nanostructure were determined by nitrogen sorption/desorption (Sorbtometer-M, Catacon, Russia) in relative pressure range 0.05 to 0.35. Zeta potential measurements were performed using Zetasizer Nano ZSP instrument equipped with an auto-titration unit MPT-2 (Malvern Instruments Ltd, GB) with use of Zetasizer Software.

Synthesis AlOOH/AlFe micro/nanostructures

Hierarchical AlOOH/AlFe micro/nanostructures were synthesized by direct reaction of an Al/Fe nanopowder with water described in Svarovskaya et al. (2015) and Bakina et al. (2020). In a typical synthesis, 4.00 g of nanopowder was placed in a reactor with 400 mL of water, stirred, and heated to 60 °C for 3 h with constant bubbling with air. The reaction products were separated by centrifugation and dried at 100 °C for 4 h.

Adsorption experiments

A sodium arsenate stock solution (500 mg As(V)/L) was prepared and the solutions with a lower concentration were prepared by subsequent dilution of the stock solution. All kinetics tests were performed at a constant temperature 25 °C. Fifty milligrams of AlOOH/AlFe was mixed with 50 mL of the sodium arsenate solution. The mixture was stirred at a speed of 200 rpm (mechanical shaker Biosan, Latvia) for a predetermined time. The concentration of arsenic in the solution was determined by inversion voltammetry, previously restoring As(V) to As(III). The analytical signal was measured

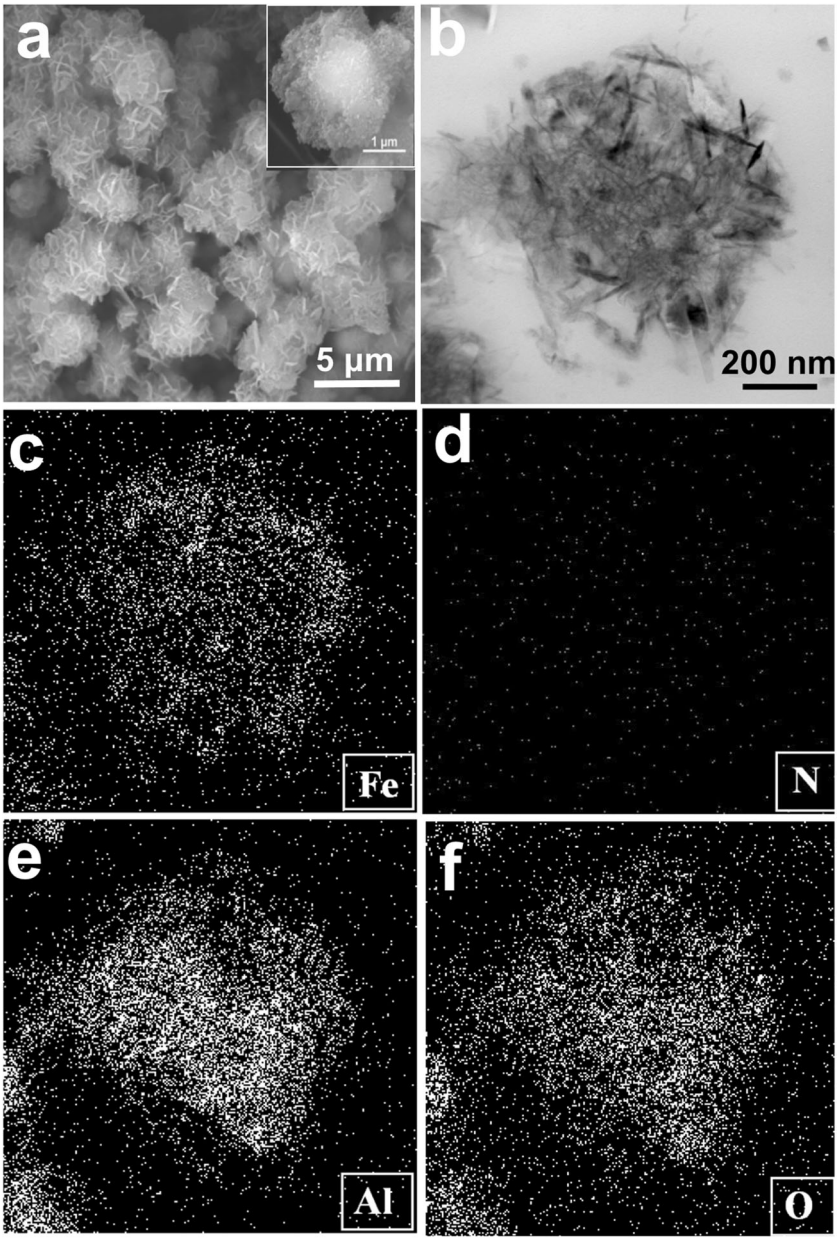

Fig. 5 SEM (**a**), TEM (**b**), EDX mapping showing the distribution of iron (**c**), nitrogen (**d**), aluminum (**e**), and oxygen (**f**) in the products of the hydrolysis of Al/Fe(N_2) nanopowder

on a voltammetric analyzer TA-2 (Tom'analit, Russia), with a two-electrode cell sensor. The measuring electrode is gold-carbon; the reference electrode is silver chloride. The background electrolyte is a solution of Trilon B 0.01 mol/L (pH 4–5). The limit of As(V) detection was 0,5 μg/L.

Before determining the concentration of the solute, the solutions were filtered through a 0.45-μm nylon membrane. The amount of arsenic adsorbed was calculated with the equation (1):

$$q_t = (C_0 - C_t) \times V/m \quad (1)$$

where q_t (mg/g) is the amount of solute sorbed per mass of sorbent at any time, C_0 and C_t (mg/L) are the concentrations of the solute at initial and any time t respectively, V is the volume of the solution (L), and m is the mass (g) of adsorbent.

In a typical adsorption experiment, 50 mg AlOOH/AlFe was respectively added into 50 mL of various solute solutions with different concentrations ranging from 0.5 to 100 mg/L under stirring for 60 min. After this the adsorbent was separated from the solution by filtration.

Equilibrium adsorption capacity q_e (mg/g) was calculated by equation (2):

$$q_e = (C_0 - C_e) \times V/m \quad (2)$$

where q_e (mg/g) is the amount of solute sorbed per mass of sorbent at equilibrium, V (L) is the volume of the solution, C_0

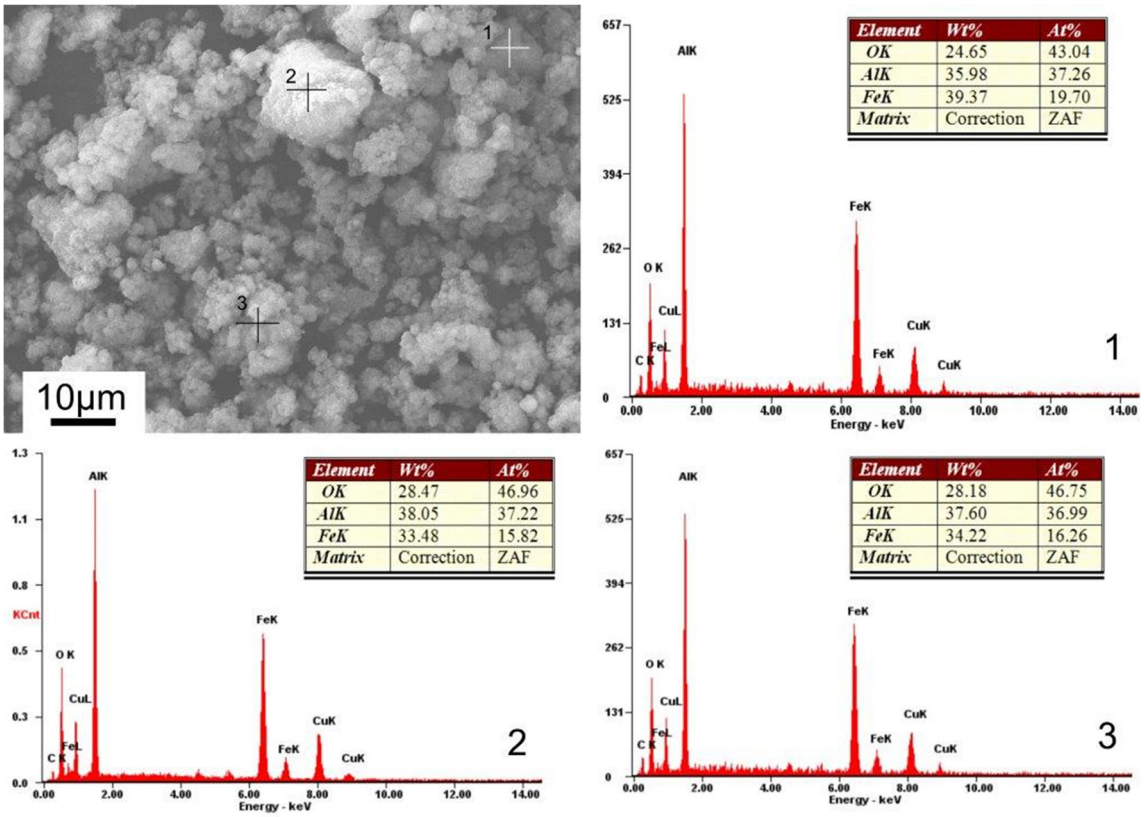

Fig. 6 SEM image of products of the hydrolysis of Al/Fe(N_2) nanopowder and their EDS spectrum

and C_e (mg/L) are initial and equilibrium concentrations of the solute, respectively, and m (g) is adsorbent weight.

Cytotoxicity assays

L929 fibroblast cell line (Vector, Russia) was used for cell viability assay. This cell line is sensitive and is often used for toxicity test. L929 cells were grown in 75-cm^2 flasks in minimum essential medium eagle supplemented with 10 wt% fetal bowline serum (HyClone) and 5 % penicillin streptomycin glutamine (HyClone) at 37 °C in a 5% CO_2 humidified atmosphere. The cells were treated with nanoparticles at concentration 10 mg/mL for 24 h, 48 h, and 72 h. After which the cell viability was determined using a standard MTT assay (Abcam).

Results and discussion

Characterization of nanoparticles and nanocomposite

The TEM and SEM images in Fig. 2 indicate that the composite bimetallic nanoparticles of Al/Fe(N_2) nanopowder are spherical in shape. The agglomerate of the nanoparticles size ranged from 0.05 to 2.0 μm, mainly from 0.2 to 0.5 μm (Fig. 3). Aluminum, iron, nitrogen, and oxygen are detected by EDS in all particles. The specific surface area of Al/Fe(N_2) nanopowder is 8 m^2/g,

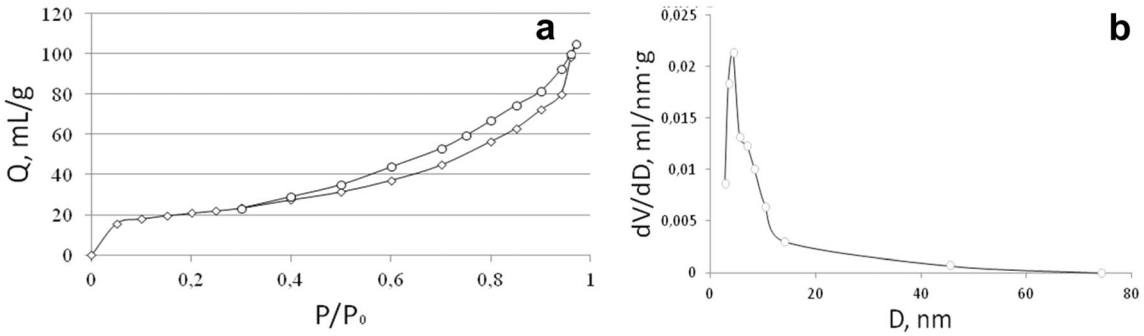

Fig. 7 Nitrogen sorption-desorption curve (**a**) and pore diameter distribution (**b**) of AlOOH/AlFe

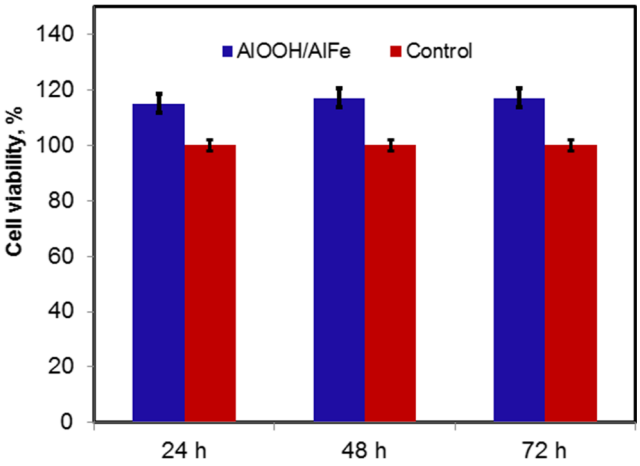

Fig. 8 In vitro toxicity AlOOH/AlFe nanocomposite

which indicates the absence of pores in the particles. Aluminum to iron ratio in the nanoparticles is not the same: along with nanoparticles whose composition is close to that of the powder as a whole (≈1:1 by weight), nanoparticles with a predominance of aluminum or iron are observed also (Fig. 2b). The uniform oxygen distribution is in good agreement with the presence of a thin passivating oxide film on the surface of powder particles as seen from the images of EDS analysis (Fig. 2f).

X-ray diffraction analysis shows that aluminum and iron in the powder are present in the form of five phases — AlFe intermetallic compound, aluminum metal, aluminum nitride, and α- and γ-phases of iron (Fig. 4a). Based on the EDS data (table on the Fig. 2a), the amount of AlN in the nanopowder is 18.68 % (wt). The remaining 25.62 % of aluminum is contained in the Al and AlFe phases.

Aluminum and aluminum nitride in the composition of the nanopowder are chemically active and react with water under mild reaction conditions (temperature from 40 °C and more and ambient pressure). The reaction is accompanied by an increase in pH value and gas evolution. The reactions are *described* with chemical *equations* (3) and (4):

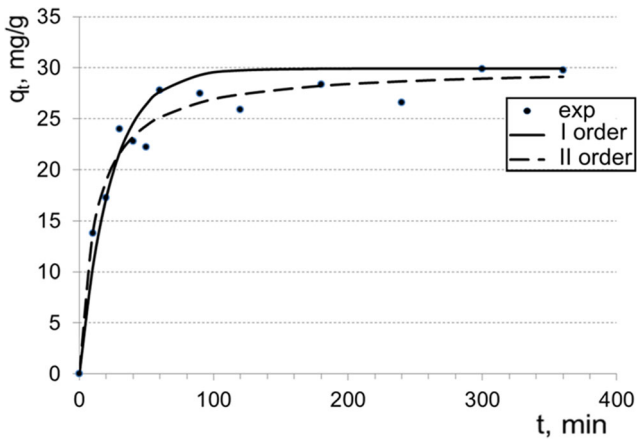

Fig. 9 Experimental and calculated kinetic curves for As(V) adsorption by AlOOH/AlFe

$$Al + H_2O = AlOOH + H_2\uparrow \quad (3)$$

$$AlN + H_2O = AlOOH + NH_3\uparrow \quad (4)$$

AlOOH formation by reactions (3) and (4) is consistent with the XRD data. In the hydrolysis products of Al/Fe(N_2) nanopowder, the phases of aluminum and aluminum nitride are not detected, but strongly broadened peaks of boehmite γ-AlOOH appear (Fig. 4b). The peaks corresponding to the AlFe intermetallic compound remain unchanged in the diffraction pattern of the reaction products, which allows us to conclude that the AlFe intermetallic compound is stable under synthesis conditions. A high-temperature γ-Fe phase stabilized in nanopowder was not detected in the reaction products, and a peak associated with the α-Fe phase of iron is observed in the diffraction pattern of the reaction product (Fig. 4b). This may mean that either the γ-Fe phase is oxidized without the formation of crystalline products, or, more likely, turns into the stable α-Fe phase. The α-Fe phase is not oxidized under synthesis conditions and is detected by the XRD method in the reaction products.

The reaction products are flower-like porous structures with a diameter in range 1–5 μm (Fig. 5). These structures consist of intersecting plates 2–5-nm thick and planar sizes from 50 to 200 nm. According to the EDS analysis, nitrogen is absent in the solid reaction products (2), but the oxygen fraction increases (Fig. 6).

Nitrogen adsorption isotherm of AlOOH/AlFe hierarchical structures

The adsorption isotherm is of type IV according to the IUPAC classification which is characteristic for mesoporous materials (Fig. 7a). The shape of the hysteresis loop in the relative pressure range p/p_0 0.3–1.0 corresponds to type H_3 according to the empirical De Boer classification indicating slit-like pores in non-rigid aggregates of plate-like particles. The pore diameter is in the range 3.5–70 nm with maximum contribution to the pore volume is made by pores with a diameter of about 5 nm (Fig. 7b). The specific surface area was 247.1 m^2/g.

As-synthesized nanostructures had low toxicity. The viability of L929 cell line increased due to contact with AlOOH/AlFe to 117.5 ± 3.3 % after 24-h exposure (Fig. 8). No significant differences in the cell viability as a function of the exposure time have been found.

Kinetics of the adsorption

The kinetics of the adsorption is one of the important characteristics. The adsorption of As(V) onto AlOOH/AlFe nanocomposite as a function of contact time at pH 7.0 and initial As(V) concentration 50 mg/L is presented in Fig. 9. Adsorption is rapid during the first 80 min and reached equilibrium after about 120 min.

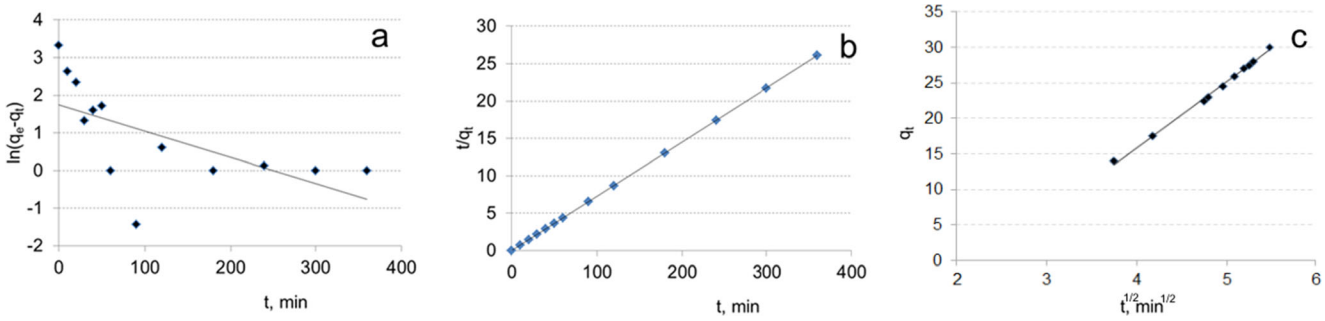

Fig. 10 Arsenic (V) adsorption kinetics by AlOOH/AlFe

The rate of adsorption in liquid-solid interactions is described with the general equation (5):

$$\frac{dq}{dt} = k(q_e - q_t)^n \tag{5}$$

where dq/dt is the rate of reaction, k is the rate constant, n is the reaction order constant rate of the pseudo-n-th order kinetic model, and q_e and q_t are the adsorbate amounts uptake per mass of adsorbent at equilibrium and at any time t, respectively.

Pseudo-first and pseudo-second-order models are widely used to describe the adsorption rate. The pseudo-first-order model is described by the equation (6):

$$\frac{dq}{dt} = k(q_e - q_t) \tag{6}$$

Integration of equation (6) taking into account the boundary conditions ($q_t = 0$ for $t = 0$, $q_t = q_e$ for $t = t$) gives the expression (7)

$$qt = qe\left(1 - e^{-kt}\right) \tag{7}$$

The pseudo-second-order model is described by the equation (8)

$$\frac{dq}{dt} = k(q_e - q_t)^2 \tag{8}$$

Integration of equation (8) taking into account the boundary conditions gives the expression (9)

$$q_t = \frac{q_e^2 kt}{1 + q_e kt} \tag{9}$$

Table 1 The kinetics parameters of arsenic adsorption on the AlOOH/AlFe surface

Parameters	Reaction order	
	I	**II**
q_e, mg/g	15.51	30.12
k	0.0154	0.089
R^2	0.724	0.995

The linear forms of the kinetics equations are of the form

$$ln(q_e - q_t) = \ln q_e - k_1 t \tag{10}$$

and

$$\frac{t}{q_t} = \frac{1}{k_2 q_e^2} + \frac{1}{q_e} t \tag{11}$$

respectively.

Figure 10 shows the graphs of the arsenic adsorption kinetics according to the pseudo-first-order (a), pseudo-second-order (b), and Weber and Morris (c) models.

The kinetics parameters of arsenic sorption by AlOOH/AlFe hierarchical micro/nanostructures were fit according to the Lagergren pseudo-first and the pseudo-second-order models (Table 1).

The determination coefficients R^2 for the pseudo-second-order model were higher than those for the first-order model, suggesting that the former better fits the experimental data (Azizian 2004). This result suggests that the adsorption rate is determined to a greater extent by the availability of adsorption centers on the adsorbent surface than by the concentration of arsenic (V) in solution.

To assess the importance of intraparticle diffusion in the kinetics of As(V) adsorption, the Weber-Morris model was applied (fig. 9). According to the model, the adsorption plot

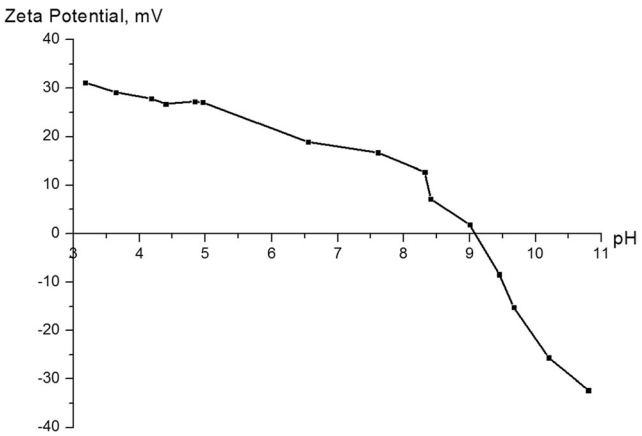

Fig. 11 pH-dependent change in the zeta potential of AlOOH/AlFe nanocomposite

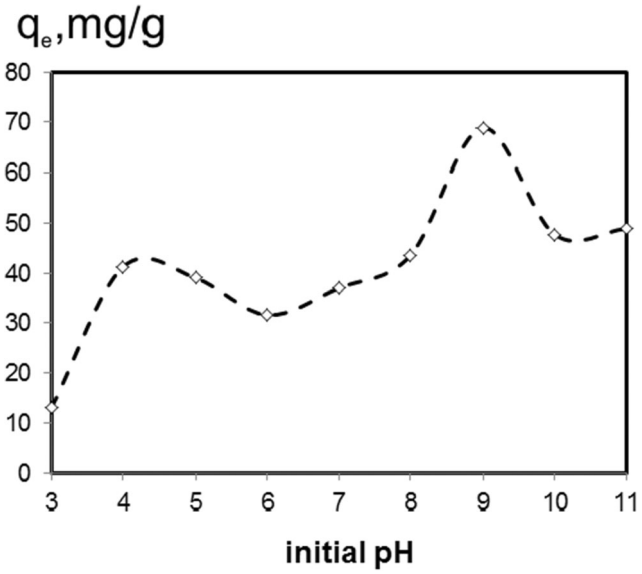

Fig. 12 Effect of initial pH of solution on As(V) adsorption (initial arsenic concentration of 50 mg/L, contact time of 60 min at 298 K)

of q_t versus the square root of contact time ($t^{1/2}$) should be linear if intraparticle diffusion is involved in the sorption process (Yusan and Erenturk 2011). Fitting the experimental data, the rectilinear section was identified, which indicates that intraparticle diffusion is the rate-controlling step.

Effect of pH

The zeta potential of hierarchical micro/nanostructures AlOOH/AlFe in the pH range of 6–8 is about + 15... + 20 mV (point zero charge pH_{pnz} = 9.3) (Fig. 11). The surface charge of nanostructures remained at pH values as low as 9.3. This should contribute to the electrostatic attraction of negatively charged species $H_2AsO_4^-$ and $HAsO_4^{2-}$, which, along with H_3AsO_4, are the main forms of As(V) at pH = 7.0 (Weidner and Ciesielczyk 2019).

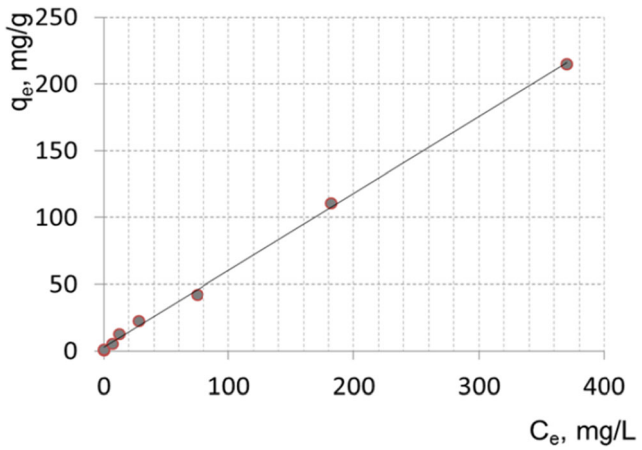

Fig. 13 Arsenic (V) adsorption isotherm by AlOOH/AlFe

Solution pH can affect both arsenate speciation and surface charge of composites and further change the As(V) sorption capacity. Experiments were carried out using initial pHs varying from 3 to 11, at constant initial arsenic concentration of 50 mg/L. The effect of pH on the As(V) adsorption capacity (q_e) is presented in Fig. 12. As(V) adsorption decreased from 12 to 43 mg/g as pH increased from 3 to 4.5 and then remained at 35–43 mg/g at pH 4.5–8. Zhang et al. (2010) has reported the increasing pH to decreasing As(V) adsorption on iron oxide surface. The higher the solution pH, the less positive charged the surface of nanostructures. The concentrations of As species are pH-dependent. At pH = 9, nanostructure surface becomes neutral and the more chemical adsorbable $HAsO_4^{2-}$ ions predominate (Huo et al. 2017). There is no electrostatic repulsion. We observed the maximum q_e = 70 mg/g. It can be concluded that an As(V) effective removal using AlOOH/AlFe nanostructures can be in wide pH range.

Adsorption isotherms

Adsorption isotherm of As(V) is shown in Figure 13. As can be seen, isotherm is of C type according to the Giles classification, indicating a high affinity of the adsorbent to the sorbate and high permeability of the sorbate. This isotherm type indicates that the number of available sorption sites is constant; the more sorbate is sorbed the more sites are created (Giles et al. 1960).

According to the experimental adsorption isotherm, 1 g of AlOOH/AlFe adsorbed more than 200 mg of arsenic, and therefore, after adsorption, it contained about 16.7 % (wt) As(V). This is in good agreement with the data of the EDS analysis of the adsorbent in a solution of arsenic with a concentration of 500 mg/L for 120 min. Figure 14 demonstrates that arsenic is fairly evenly distributed in the adsorbent and its concentration is approximately 13 % (wt).

The obtained isotherm was analyzed using common Langmuir and Freundlich adsorption models. The Langmuir model considers that the sorption energy of each molecule is the same. The monolayer capacity can be presented by the expression (12):

$$Q_e = \frac{Q_m k_L C_e}{1 + k_L C_e} \tag{12}$$

where k_L (l/mg) is the Langmuir isotherm constant, Q_e (mg/g) and C_e (mg/L) are respectively the solid phase concentration and liquid phase concentration of adsorbate at equilibrium, and Q_m (mg/g) is the maximum amount of adsorbed adsorbate per a unit weight of adsorbent.

The Freundlich isotherm has been largely used to describe solid-liquid sorption systems. The Freundlich isotherm is an empirical equation (13) employed to describe the multilayer adsorption. This model predicts that the sorbate concentration

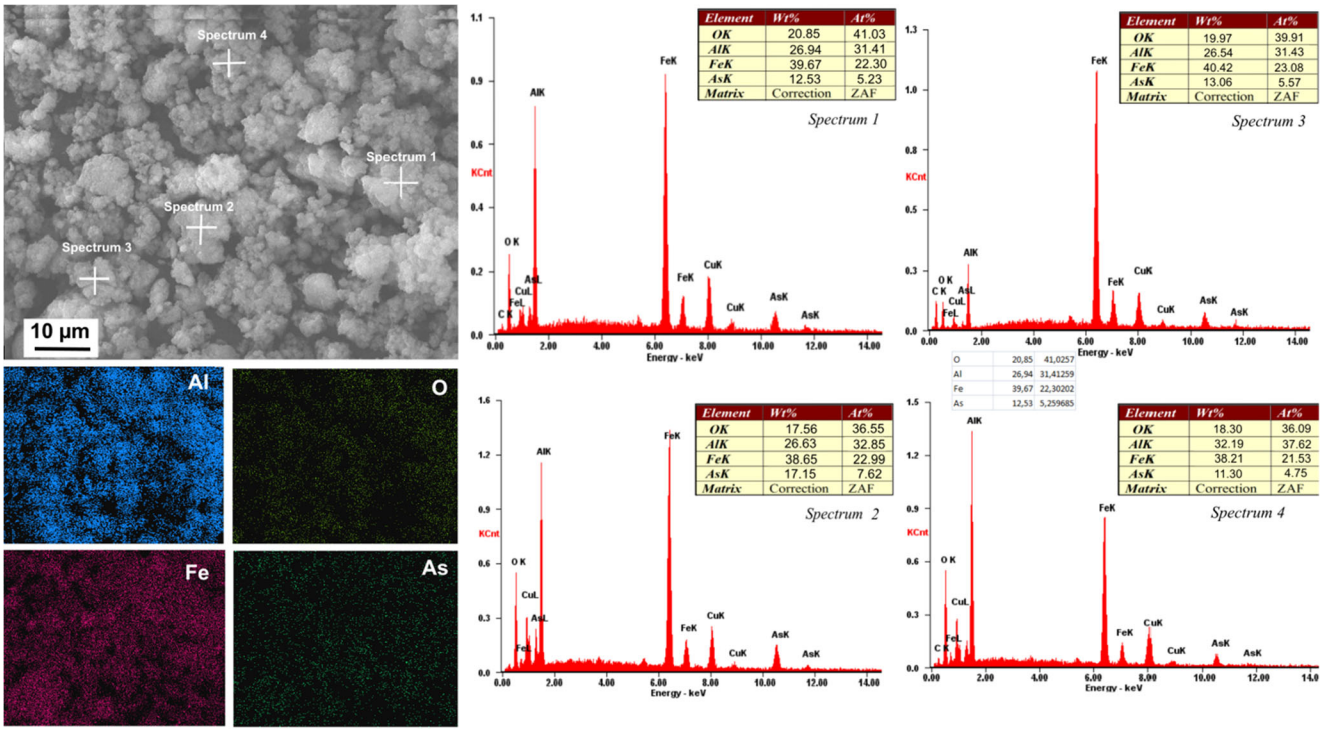

Fig. 14 SEM, EDX mapping showing the distribution of aluminum, oxygen, iron, and arsenic, as well as the EDS spectrum and the quantitative content of elements in AlOOH/AlFe after sorption of arsenic

on the adsorbent will increase with the increase of the adsorbate concentration in the solution. This model is applied in reversible adsorption onto heterogeneous surfaces.

$$Q_e = k_F C_e^{\frac{1}{n}} \tag{13}$$

where k_F — Freundlich constant and n — a dimensionless Freundlich constant.

The magnitude of $n_F = 1/n$ quantifies the favorability of adsorption and the degree of heterogeneity of the surface.

The linearized forms of the Langmuir (12) and Freundlich (13) equations and graphs are shown in Fig. 15.

A good agreement between the experimental data and the Freundlich model indicates multilayer adsorption on an energetically inhomogeneous adsorbent surface. Arsenic adsorption by this mechanism was observed on manganese ferrite nanoparticles (Martinez–Vargas et al. 2018), iron-doped chitosan microsphere (Lin et al. 2019), and magnetic nanoparticles Fe_3O_4 decorated with β-cyclodextrins-functionalized graphene oxide (Kumar and Jiang 2017). Thus, As(V) can be successfully adsorbed by nanostructured AlOOH/AlFe, which was not previously used for this.

Comparison of the data obtained in this work with the works of other authors is given in Table 2.

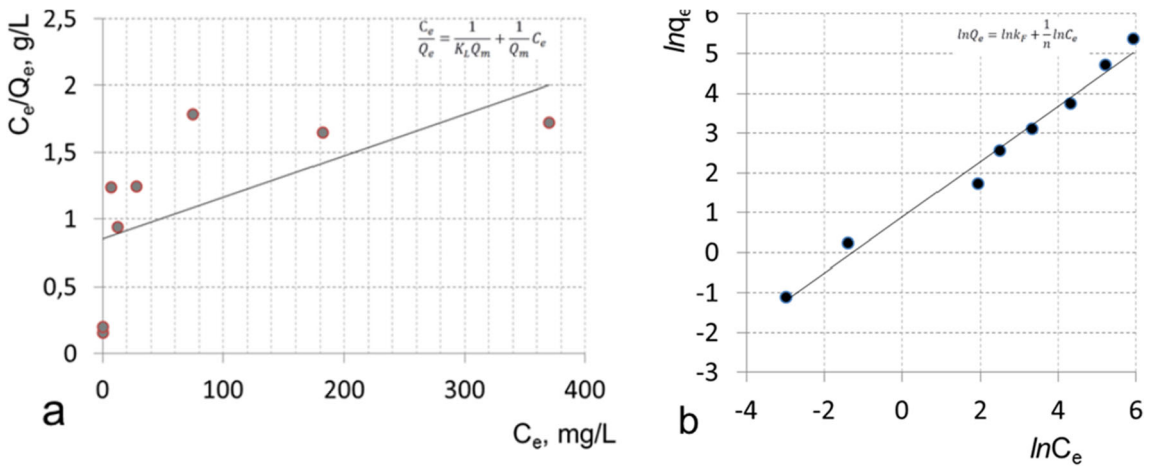

Fig. 15 Linearized Langmuir (**a**) and Freundlich (**b**) adsorption isotherm

Table 2 Arsenic (V) adsorption of porous iron-based nanocomposites

Nanocomposites	Synthesis method	Specific surface area, m^2/g	Maximum capacity (mg/g) As(V)	References
Fe_2O_3-Mn_2O_3	Aeration-co-precipitation method	244.79	15 mg/g of coagulant	Eslami et al. (2020)
Clay/Fe-Mn composite	Fe and Mn salts-modified natural clay	55.45	120.70 mg/g	Foroutan et al. (2019)
Lanthanum-modified iron oxide	Commercial iron-based sorbent modified by lanthanum(III)	–	61.97 mg/g	Dudek and Kołodyńska (2020)
Graphene oxide (GO), iron-modified clinoptilolite	Co-precipitation method	–	0,557 mg/g	Baskan and Hadimlioglu (2021)
Ce(IV)-doped iron oxide	Co-precipitation method	–	70.4 mg/g	Zhang et al. (2003)
Sulfur-doped Fe_3O_4 nanoparticles	Low-temperature mixing and high-temperature sintering	–	58,38 mg/g	Liu et al. (2018)
$Fe_2O_3/La_2O_2CO_3$ composites	Calcined metal-organic frameworks under air at 550 °C (with a heating rate of 5 °C/min) for 5 h	34.3	410 mg/g at La mass ratio 11 %	Huo et al. (2020)
AlOOH/AlFe	EEW		More than 200 mg/g	In present research

Our studies have shown that the adsorption capacity of AlOOH/AlFe nanostructures is similar to lanthanum-modified iron oxide nanoparticles.

Conclusion

This study addressed the potential of AlOOH/AlFe hierarchical micro/nanostructures for As(V) adsorption from aqueous solutions as an example. The flower-shape AlOOH morphology not only facilitated deliverability, but increased the As(V) sorption capacity by up to 200 mg/g.

The adsorption kinetics has been found to be described by a pseudo-second-order equation of Lagergren and Weber-Morris models while the experimental adsorption isotherm is closest to the Freundlich model. This indicates the energy heterogeneity of the adsorbent surface and multilayer adsorption. Fast adsorption and high sorption capacity show that the particles can be applied in a device to continuously treat arsenic-polluted water in wide pH range. The possibility of magnetic separation and mild synthesis conditions allow to avoid the use of sophisticated equipment for hydrothermal treatment, filtration, or high-speed centrifugation.

Author contribution All authors contributed to the study conception and design. Material preparation, data collection, and analysis were performed by Svarovskaya N.V. and Bakina O.V. The first draft of the manuscript was written by Svarovskaya N.V. and all authors commented on previous versions of the manuscript. Glazkova E.A. studied physical and chemical properties of nanoparticles and nanostructures. Rodkevich N. performed the adsorption computations. Lerner M. obtained nanoparticles by electrical explosive of wires. Vornakova E. and Chzhou V. performed the adsorption experiments. Naumova L. contributed to the interpretation of the results. All authors read and approved the final manuscript.

Funding The work was performed according to the government research assignment for ISPMS SB RAS, project FWRW-2019-0033.

Data Availability All data and materials are available.

Declarations

Ethics approval Not applicable, because this article does not contain any studies with human or animal subjects.

Consent to participate All authors consent to participate in a study.

Consent for publication All authors consent to publish their data in a journal article.

Conflict of interest The authors declare no competing interests.

References

Ali I (2012) New generation adsorbents for water treatment. Chem Rev 112(10):5073–5091. https://doi.org/10.1021/cr300133d

Alka S, Shahir S, Ibrahim N, Ndejiko MJ, Vo DVN, Abd Manan F (2020) Arsenic removal technologies and future trends: a mini review. J Clean Prod 123805:123805. https://doi.org/10.1016/j.jclepro.2020.123805

Azizian S (2004) Kinetic models of sorption: a theoretical analysis. J Colloid Interface Sci 276(1):47–52. https://doi.org/10.1016/j.jcis.2004.03.048

Bakina OV, Svarovskaya NV, Glazkova EA, Lozhkomoev AS, Khorobraya EG, Lerner MI (2015) Flower-shaped ALOOH nanostructures synthesized by the reaction of an AlN/Al composite nanopowder in water. Adv Powder Technol 26(6):1512–1519. https://doi.org/10.1016/j.apt.2015.08.007

Bakina OV, Glazkova EA, Lozhkomoev AS, Svarovskaya NV, Rodkevich NG, Lerner MI (2020) Synthesis and antibacterial activity of cellulose acetate sheets modified with flower-shaped AlOOH/Ag. Cellulose 27:6663–6676. https://doi.org/10.1007/s10570-020-03250-2

Baskan MB, Hadimlioglu S (2021) Removal of arsenate using graphene oxide-iron modified clinoptilolite-based composites: adsorption kinetic and column study. J Anal Sci Technol 12(1):1–16. https://doi.org/10.1186/s40543-021-00274-6

Cai W, Duan G, Li Y (2014) Hierarchical micro/nanostructured materials: fabrication, properties, and applications. CRC Press, London. https://doi.org/10.1201/b17075

Dubey SP, Dwivedi AD, Sillanpaa M et al (2017) Adsorption of As (V) by boehmite and alumina of different morphologies prepared under hydrothermal conditions. Chemosphere 169:99–106. https://doi.org/10.1016/j.chemosphere.2016.11.052

Dudek S, Kołodyńska D (2020) Enhanced Arsenic (V) Removal on an iron-based sorbent modified by lanthanum (III). Materials 13(11): 2553. https://doi.org/10.3390/ma13112553

Ecer Ü, Yılmaz Ş, Şahan T (2018) Highly efficient Cd (II) adsorption using mercapto-modified bentonite as a novel adsorbent: an experimental design application based on response surface methodology for optimization. Water Sci Technol 78(6):1348–1360. https://doi.org/10.2166/wst.2018.400

Eslami H, Ehrampoush MH, Esmaeili A, Ebrahimi AA, Salmani MH, Ghaneian MT, Falahzadeh H (2018) Efficient photocatalytic oxidation of arsenite from contaminated water by Fe_2O_3-Mn_2O_3 nanocomposite under UVA radiation and process optimization with experimental design. Chemosphere 207:303–312. https://doi.org/10.1016/j.chemosphere.2018.05.106

Eslami H, Ehrampoush MH, Esmaeili A, Salmani MH, Ebrahimi AA, Ghaneian MT, Fard RF (2019a) Enhanced coagulation process by Fe-Mn bimetal nano-oxides in combination with inorganic polymer coagulants for improving As (V) removal from contaminated water. J Clean Prod 208:384–392. https://doi.org/10.1016/j.jclepro.2018.10.142

Eslami H, Ehrampoush MH, Esmaeili A, Ebrahimi AA, Ghaneian MT, Falahzadeh H, Salmani MH (2019b) Synthesis of mesoporous Fe-Mn bimetal oxide nanocomposite by aeration co-precipitation method: physicochemical, structural, and optical properties. Mater Chem Phys 224:65–72. https://doi.org/10.1016/j.matchemphys.2018.11.067

Eslami H, Esmaeili A, Ehrampoush MH, Ebrahimi AA, Taghavi M, Khosravi R (2020) Simultaneous presence of poly titanium chloride and Fe_2O_3-Mn_2O_3 nanocomposite in the enhanced coagulation for high rate As (V) removal from contaminated water. J Water Process Eng 36:101342. https://doi.org/10.1016/j.jwpe.2020.101342

Foroutan R, Mohammadi R, Adeleye AS, Farjadfard S, Esvandi Z, Arfaeinia H, Sahebi S (2019) Efficient arsenic (V) removal from contaminated water using natural clay and clay composite adsorbents. Environ Sci Pollut Res 26(29):29748–29762. https://doi.org/10.1007/s11356-019-06070-5

Giles CH, MacEwan TH, Nakhwa SN, Smith D (1960) Studies in adsorption. Part XI. A system of classification of solution adsorption isotherms, and its use in diagnosis of adsorption mechanisms and in measurement of specific surface areas of solids. J Chem Soc 111: 3973–3993. https://doi.org/10.1039/jr9600003973

Guo L, Ye P, Wang J, Fu F, Wu Z (2015) Three-dimensional Fe3O4-graphene macroscopic composites for arsenic and arsenate removal. J Hazard Mater 298:28–35. https://doi.org/10.1016/j.jhazmat.2015.05.011

Guo Q, Cao Y, Yin Z, Yu Z, Zhao Q, Shu Z (2017) Enhanced removal of arsenic from water by synthetic nanocrystalline iowaite. Sci Rep 7(1):17546. https://doi.org/10.1038/s41598-017-17903-z

Habuda-Stanić M, Nujić M (2015) Arsenic removal by nanoparticles: a review. Environ Sci Pollut Res 22(11):8094–8123. https://doi.org/10.1007/s11356-015-4307-z

Huo L, Zeng X, Su S, Bai L, Wang Y (2017) Enhanced removal of As (V) from aqueous solution using modified hydrous ferric oxide nanoparticles. Sci Rep 7(1):1–12. https://doi.org/10.1038/srep40765

Huo JB, Gupta K, Lu C, Hansen HCB, Fu ML (2020) Recyclable high-affinity arsenate sorbents based on porous Fe_2O_3/$La_2O_2CO_3$ composites derived from Fe-La-C frameworks. Colloids Surf A Physicochem Eng Asp 585:124018. https://doi.org/10.1016/j.colsurfa.2019.124018

Kang BK, Lim BS, Yoon Y, Kwag SH, Park WK, Song YH, Yang WS, Ahn YT, Kang JW, Yoon DH (2017) Efficient removal of arsenic by strategically designed and layer-by-layer assembled PS@+rGO@GO@Fe_3O_4 composites. J Environ Manag 201:286–293. https://doi.org/10.1016/j.jenvman.2017.05.066

Kumar ASK, Jiang SJ (2017) Synthesis of magnetically separable and recyclable magnetic nanoparticles decorated with β-cyclodextrin functionalized graphene oxide an excellent adsorption of As (V)/(III). J Mol Liq 237:387–401. https://doi.org/10.1016/j.molliq.2017.04.093

Lerner MI, Pervikov AV, Glazkova EA, Svarovskaya NV, Lozhkomoev AS, Psakhie SG (2016) Structures of binary metallic nanoparticles produced by electrical explosion of two wires from immiscible elements. Powder Technol 288:371–378. https://doi.org/10.1016/j.powtec.2015.11.037

Li G, Lan J, Liu J, Jiang G (2013) Synergistic adsorption of As (V) from aqueous solution onto mesoporous silica decorated orderly with Al_2O_3 and Fe_2O_3 nanoparticles. J Colloid Interface Sci 405:164–170. https://doi.org/10.1016/j.jcis.2013.05.055

Li Z, Wang L, Meng J, Liu X, Xu J, Wang F, Brookes P (2018) Zeolite-supported nanoscale zero-valent iron: new findings on simultaneous adsorption of Cd (II), Pb (II), and As (III) in aqueous solution and soil. J Hazard Mater 344:1–11. https://doi.org/10.1016/j.jhazmat.2017.09.036

Lin X, Wang L, Jiang S, Cui L, Wu G (2019) Iron-doped chitosan microsphere for As (III) adsorption in aqueous solution: kinetic, isotherm and thermodynamic studies. Korean J Chem Eng 36(7):1102–1114. https://doi.org/10.1007/s11814-018-0117-6

Liu J, Kong L, Huang X, Liu M, Li L (2018) Removal of arsenic (V) from aqueous solutions using sulfur-doped Fe_3O_4 nanoparticles. RSC Adv 8(71):40804–40812. https://doi.org/10.1039/C8RA08699K

Martinez–Vargas S, Martinez AI, Hernandex-Beteta EE et al (2018) As (III) and As (V) adsorption on manganese ferrite nanoparticles. J Mol Struct 1154:524–534. https://doi.org/10.1016/j.molstruc.2017.10.076

Mikhaylov VI, Maslennikova TP, Krivoshapkin PV (2017) Characterization and sorption properties of γ-AlOOH/α-Fe2O3 composite powders prepared via hydrothermal method. Mater Chem Phys 186:612–619. https://doi.org/10.1016/j.matchemphys.2016.11.044

Peng X, Zhao Y, Yang Y et al (2018) One-step and acid free synthesis of γ-Fe2O3/SBA-15 for enhanced arsenic removal. Microporous Mesoporous Mater 258:26–32. https://doi.org/10.1016/j.micromeso.2017.08.050

Ren Z, Guo Y, Liu C, Gao PX (2013) Hierarchically nanostructured materials for sustainable environmental applications. Front Chem 1:18. https://doi.org/10.3389/fchem.2013.00018

Seino S, Kusunose T, Sekino T, Kinoshita T, Nakagawa T, Kakimi Y, Mizukoshi Y (2006) Synthesis of gold/magnetic iron oxide composite nanoparticles for biomedical applications with good dispersibility. J Appl Phys 99(8):08H101. https://doi.org/10.1063/1.2151826

Shakoor MB, Nawaz R, Hussain F, Raza M, Ali S, Rizwan M, Oh SE, Ahmad S (2017) Human health implications, risk assessment and remediation of As-contaminated water: a critical review. Sci Total Environ 601:756–769. https://doi.org/10.1016/j.scitotenv.2017.05.223

Svarovskaya NV, Berenda AV, Bakina OV, Glazkova EA, Lozhkomoev AS, Khorobraya EG, Fomenko AN (2015) Chemical behaviour of Al/Cu nanoparticles in water. Prog Nat Scie 25(1):1–5. https://doi.org/10.1016/j.pnsc.2015.01.001

Weidner E, Ciesielczyk F (2019) Removal of hazardous oxyanions from the environment using metal-oxide-based materials. Materials 12(6): 927. https://doi.org/10.3390/ma12060927

Yılmaz Ş, Ecer Ü, Şahan T (2018) Modelling and optimization of As (III) adsorption onto thiol-functionalized bentonite from aqueous solutions using response surface methodology approach. Chemistry Select 3(32):9326–9335. https://doi.org/10.1002/slct.20180

Yusan SD, Erenturk SA (2011) Sorption behaviors of uranium (VI) ions on α-FeOOH. Desalination 269(1-3):58–66. https://doi.org/10.1016/j.desal.2010.10.042

Zhang Y, Yang M, Huang X (2003) Arsenic (V) removal with a Ce (IV)-doped iron oxide adsorbent. Chemosphere 51(9):945–952. https://doi.org/10.1016/S0045-6535(02)00850-0

Zhang K, Dwivedi V, Chi C, Wu J (2010) Graphene oxide/ferric hydroxide composites for efficient arsenate removal from drinking water. J Hazard Mater 182(1-3):162–168. https://doi.org/10.1016/j.jhazmat.2010.06.010

Zhang P, O'Connor D, Wang Y, Jiang L, Xia T, Wang L, Hou D (2020) A green biochar/iron oxide composite for methylene blue removal. J Hazard Mater 384:121286. https://doi.org/10.1016/j.jhazmat.2019.121286

Zhong LB, Liu Q, Zhu JQ, Yang YS, Weng J, Wu P, Zheng YM (2018) Rational design of 3D urchin-like FeMnxOy@FeOOH for water purification and energy storage. ACS Sustain Chem Eng 6(3): 2991–3001. https://doi.org/10.1021/acssuschemeng.7b02689

Zhu J, Zhu Z, Zhang H, Lu H, Zhang W, Qiu Y, Zhu L, Küppers S (2018) Calcined layered double hydroxides/reduced graphene oxide composites with improved photocatalytic degradation of paracetamol and efficient oxidation-adsorption of As (III). Appl Catal B Environ 225:550–562. https://doi.org/10.1016/j.apcatb.2017.12.003